Estuarine, Coastal and Shelf Science 286 (2023) 108342

Contents lists available at ScienceDirect

Estuarine, Coastal and Shelf Science

journal homepage: www.elsevier.com/locate/ecss

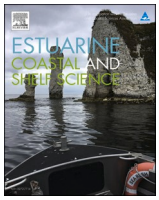

High-frequency zones of phytoplankton blooms in the Río de la Plata Estuary associated with El Niño-Southern Oscillation

Bernardo Zabaleta [a,b,*], Signe Haakonsson [b], Marcel Achkar [a], Luis Aubriot [b]

[a] Laboratorio de Desarrollo Sustentable y Gestión Ambiental del Territorio, Instituto de Ecología y Ciencias Ambientales, Facultad de Ciencias, Universidad de la República, Montevideo, Uruguay
[b] Grupo de Ecología y Fisiología de Fitoplancton, Sección Limnología, Instituto de Ecología y Ciencias Ambientales, Facultad de Ciencias, Universidad de la República, Montevideo, Uruguay

ARTICLE INFO

Keywords:
Remote sensing
Eutrophication
Water quality monitoring
Chlorophyll-*a*
Sentinel-2

ABSTRACT

In recent decades, the Río de la Plata Estuary has shown an increase in the frequency and intensity of phytoplankton blooms with negative impacts on production activities, human health, and biodiversity. Water quality monitoring programs provide samples from the coastal zone alone, which limits the collection of data inside the Estuary and the analysis of the spatio-temporal dynamics of phytoplankton blooms, as well as their relationship with flow rate. In this work, a systematic satellite monitoring of the Estuary was carried out for the first time. Sentinel-2 images captured during 2016–2021 were used along with the Normalized Difference Chlorophyll Index. It included one year of El Niño, one neutral year and two consecutive years of La Niña. Four zones with the highest frequency of bloom occurrence were delimited. Data on the extent and intensity in which blooms occurred were extracted and related to the flow rates of the main tributaries using Bayesian models. The most intense and frequent blooms were detected on the southern and northern coasts, respectively (maximum values of 515 km^2 in January 2021, NDCI>0.06), followed by a wide area of intense phytoplankton development inside the Estuary. Blooms were more frequent in warmer months, with elevated Chl-*a* concentrations in 75% of the months of the study period on the Argentine coast, and 50% on the Uruguayan coast. Blooms were positively correlated with low flows. Therefore, the most extensive and intense bloom episodes occur during La Niña events. During El Niño, the high flows transport the biomass originating in the Estuary and in the hydroelectric reservoirs located upstream, which can even be transported along the northern coast. This work identified a recurrent pattern of phytoplankton blooms and the hydro-meteorological conditions that favor their magnification in a context of strong climate variability in the region and estuarine eutrophication.

1. Introduction

In recent decades, the occurrence and intensity of harmful algal blooms (HABs) in both freshwater and marine ecosystems have intensified (O'Neil *et al.*, 2012; Burford et al., 2020). This phenomenon impacts the trophic web, biodiversity, and water quality, as these blooms can also produce several toxins that are harmful to health (Chorus and Welker, 2021). In addition to the risk to public health and the degradation of landscape value, the HABs can exacerbate economic loss by affecting tourism and production activities (Carpenter et al., 1998; Conley et al., 2009; Dodds et al., 2009; Chapin et al., 2011).

Estuaries are frequently affected by HABs, both marine and freshwater, for being transition zones between rivers and oceans, and strongly impacted by anthropogenic activities and climate variability. They are characterized by a great spatial variability, with important gradients of turbidity, salinity, temperature, nutrient fluxes, and hydrological patterns, making them one of the most productive habitats in the world (Mitchell et al., 2015; Muniz et al., 2019). While meteorological conditions determine estuarine circulation and residence times, as well as the magnitude and timing of river discharges (Hardisty, 2007), anthropogenic activities from the mainland contribute dissolved organic matter, particulate matter, nutrients, and HABs in some cases (Michalak, 2016; Aubriot et al., 2020). The overgrowth of these organisms is characterized by high spatio-temporal heterogeneity in estuaries (Bowling et al., 2015). In large estuaries, in particular, it is difficult to study HABs using traditional monitoring systems. Numerous samplings

* Corresponding author. Facultad de Ciencias, Universidad de la República, Iguá 4225, CP11400, Montevideo, Uruguay.
E-mail address: bzabaleta@fcien.edu.uy (B. Zabaleta).

https://doi.org/10.1016/j.ecss.2023.108342
Received 23 December 2022; Received in revised form 11 April 2023; Accepted 17 April 2023
Available online 19 April 2023

are needed to cover estuarine spatio-temporal heterogeneity and considerable financial efforts, time, and qualified specialists are required (Navalgund et al., 2007; Lins et al., 2017).

With traditional monitoring, sampling stations are located in coastal areas in order to repeat data collection on a frequent basis. This introduces important limitations for interpreting what happens inside the water body, and makes it difficult to describe the spatio-temporal dynamics of HABs (Tamm et al., 2019). This fact is further exacerbated during large bloom events as changes in communities are often rapid and can have spatial variability of chlorophyll-a, especially in the case of cumulative blooms (e.g., *Microcystis*) (Chorus and Welker, 2021). This type of bloom can form tight clusters of high concentrations and go unnoticed in spatially constrained sampling (Oliver et al., 2012; Bowling et al., 2015). In this regard, it is critical to count on methods capable of monitoring large water bodies synoptically and with high frequency (Smayda, 1998; Anderson et al., 2001; Gallegos and Neale, 2015).

For more than four decades now, remote sensing has been used as an alternative tool for the assessment of phytoplankton pigments and suspended solid concentrations, mainly focusing on oceans, estuaries, and large lakes (Strong, 1974; Gordon et al., 1980; Gitelson et al., 1986; Gons, 1999; Nechad et al., 2010). Its greatest potential lies in the decrease in monitoring costs with respect to traditional methodologies. The availability of time series data, the possibility of monitoring wide surfaces and a large number of water bodies, as well as of estimating water quality on a regular basis (Ritchie et al., 2003; Page et al., 2018) are some of the main advantages. On the other hand, the disadvantages of remote sensing with regard to monitoring phytoplankton are taxonomic resolution, the inability to detect blooms not located in surface waters, turbidity interference, among others (Mishra and Mishra, 2014; Kutser et al., 2016).

Among the most developed approaches to satellite estimation of phytoplankton biomass by chlorophyll-*a* (Chl-*a*) concentration in optically complex waters such as estuaries, the reflectance ratio between the red (~665 nm) and red-edge (~700 nm) bands should be highlighted (Gitelson, 1992; Gons et al., 2002). Schalles and Hladik (2012) explored approaches for estimating Chl-*a* concentration from censored reflectance in a wide range of estuarine and coastal water conditions, and obtained the most accurate results for indicators considering near-red and red-edge reflectance even under highly variable conditions of colored dissolved organic matter (CDOM) and suspended solids. Mishra and Mishra (2012) developed the Normalized Difference Chlorophyll Index (NDCI) from the red-red edge ratio, which has been successfully validated in optically complex waters (Augusto-Silva et al., 2014; Beck et al., 2016; Page et al., 2018). Its use also allowed to learn about the origin of a massive cyanobacteria bloom in the Río de la Plata Estuary (RdlP) (Aubriot et al., 2020).

Currently, numerous satellite provides free multispectral images, including the Multi Spectral Instrument (MSI) sensor on board the Sentinel-2 satellite (2015) of the European Space Agency (ESA). Sentinel-2 aims to contribute to the monitoring of coastal and continental areas by providing images with a frequency of 5 days, a 100 km by 100 km squared tile, and 13 bands with one centered at 705 nm that allows estimating Chl-*a* concentration (Kutser et al., 2016; Liu et al., 2017; Dörnhöfer et al., 2018). Also, their spatial resolution (10, 20, and 60 m) allows for an accurate assessment of concentrations, which is especially useful in coastal monitoring or for detecting cumulative blooms (Toming et al., 2016).

The RdlP is a highly complex region that encompasses broad physicochemical gradients that result in a dynamic and unique system (Framiñan and Brown, 1996; Acha et al., 2008). It is characterized by a turbidity front, which divides the continental waters from the oceanic shelf; and its location varies during the year depending on the wind and the estuarine flow which is mainly determined by the flow of the Paraná River (RP), followed by the Uruguay River (RU) and, to a lesser extent, the Negro River (RN) (Muniz et al., 2019; Maciel et al., 2021). The Estuary has shown symptoms of eutrophication favored by the construction of large hydroelectric dams located in its basin such as Yacyretá, Itaipú, Salto Grande, Palmar, Rincón del Bonete, as well as by the expansion of agricultural lands, pollution of point sources due to urbanization and industrialization, and strong climate variability (Nagy et al., 2002, 2014; Brugnoli et al., 2019; Muniz et al., 2019; Aubriot et al., 2020). One of the most notorious symptoms of eutrophication is the frequent HABs recorded on the northern and southern shores of the RdlP. Particularly, cyanobacteria blooms have been monitored on the beaches of Montevideo during the last two decades (De Leon and Yunes, 2001; Pírez et al., 2013), as well as on the southern Argentine coast (Andrinolo et al., 2007; Giannuzzi et al., 2012; Sathicq et al., 2014). However, there is scarce information on the phenomenon of phytoplankton blooms at the estuarine level, and, in particular, the existence of areas with a higher frequency of occurrence of this phenomenon and its relationship with the main hydrometeorological forcings have not been evaluated so far.

During El Niño-Southern Oscillation (ENSO) phenomenon, the flow of the main tributaries increases, leading to significant changes in the RdlP (Camilloni and Barros, 2000). Particularly, salinity, the location of the turbidity front, nutrient availability, and phytoplankton biomass vary (Nagy et al., 2002). During such an event and for short periods of time the RU can reach peak flows approaching those of the RP (Brugnoli et al., 2019). In the summer of 2019, this behavior favored the largest discharge of phytoplankton biomass recorded so far, which was formed by the *Microcystis* complex and reached the Atlantic Ocean coast (Kruk et al., 2019). This phenomenon developed mainly in the hydroelectric production reservoirs of the RN and the high flows of the main tributary rivers transported it to the RdlP (Aubriot et al., 2020).

During the low flow of the RdlP associated with La Niña phase, higher phytoplankton biomass belonging to cyanobacteria have been reported in Argentine coast (Sathicq et al., 2014). Diatom (e.g. of the genera *Skeletonema*) and chlorophyte blooms were reported during La Niña and El Niño, respectively, mainly in spring (Sathicq et al., 2014). Blooms of noxious dinoflagellates (e.g of the genera *Alexandrium*) affects mainly the external zone of the Estuary (FREPLATA, 2005). The occurrence of blooms have progressively increased in recent decades and throughout the year with the exception of winter (Gómez, 2014). In particular, this phenomenon could be influenced by the historical low water levels recently recorded in the RP (Naumann et al., 2021).

Phytoplankton blooms are frequently monitored through Sentinel-2 images, we highlight the experience in the Guadiana Estuary (Spain and Portugal), where Caballero et al. (2020) estimated the duration, extension, and dynamics of a HAB. Lins et al. (2017) monitored Chl-a with high precision in a tropical estuarine-lagoon system in Brazil. In the RdlP remote sensing has been used mainly to assess the spatio-temporal dynamics of the turbidity front (Dogliotti et al., 2016; Maciel et al., 2021). However, there is a lack of studies which evaluate eutrophication processes. In this context, the present work sought to detect areas of a high frequency of phytoplankton bloom's occurrence in the middle zone of the RdlP and to evaluate their relationship with the variability of the flow rates of the RP, RU and RN associated with the ENSO phenomenon.

2. Methodology

The methodological strategy comprised four sections. In the first one, satellite imagery and the NDCI indicator were obtained (Fig. 1). The second section aimed to spatially and temporally evaluate phytoplankton blooms in the middle Estuary and part of the outer zone. For this purpose, frequency maps were produced and zonation was obtained based on MSI/Sentinel-2 image series processing between November 2016 and July 2021. The third section sought to obtain flow information and NDCI zonal statistics on all the downloaded images. The fourth section was centered on identifying ratios between phytoplankton blooms and flow rates in the RP, RU and RN, for which a Bayesian regression model was constructed (Fig. 1).

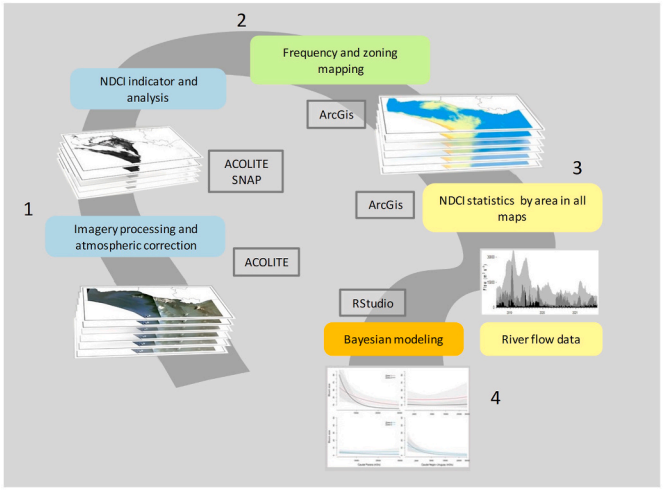

Fig. 1. Methodological strategy. Different stages are identified with numbers and colors. The software used in each stage is specified in the rectangles. (For interpretation of the references to color in this figure legend, the reader is referred to the Web version of this article.)

2.1. Study area

The Río de la Plata Estuary basin is the fifth largest in the world. It covers five South American countries and has nearly 160 million inhabitants. Its basin covers an area of 3,170,000 km^2, which represents 1/6 of the continent, and it is the second largest basin. It has two major tributaries, the Paraná and the Uruguay rivers (Muniz et al., 2019). On the northern Uruguayan coast, it extends from the Department of Colonia to Punta del Este, Maldonado (outer limit) (Fig. 2), where several economic activities are carried out, such as artisanal fishing and tourism. In addition, the northern coast is the entrance to the La Plata River basin (García-Alonso et al., 2019). On the southern coast, the basin extends from the Argentine province of Entre Ríos to the Punta Rasa of Cape San Antonio (outer limit).

Daily flow data from RP was obtained from the National Water and Sewer Institute, Argentina (INA) at Rosario city (32°58′22.04″ S, 60°37′5.50″ W). Daily RU flow from INA at Concordia city (31°24′15.61″S, 58° 0′15.38″W), and from RN at Mercedes city (33°14′45.37″ S, 58° 2′17.49″ W) provided by the National Administration of Industry and Electric Transmissions, Uruguay (UTE) (Fig. 2).

2.2. Obtaining and processing of satellite information

In order to analyze the spatial distribution of phytoplankton blooms in the RdlP, according to the availability of MSI/Sentinel-2 images, all images between November 2016 and July 2021 with low cloud cover were downloaded from https://earthexplorer.usgs.gov/. Specifically, 2 image grids with codes T21HVB and T21HWB were used (Fig. 2). Then, the presence/absence of blooms in each image was determined in the ESA's Sentinel Applications Platform (SNAP), using the NDCI>0 values as a criterion to determine Chl-*a* presence. Said criterion was determined according to the research of Caballero et al. (2020) carried out in optically complex waters. Also, in line with the adjustment obtained by Mishra et al. (2018) and subsequently applied by Aubriot et al. (2020) in the RdlP Estuary, a NDCI = 0 value corresponding to approximately 14 μg Chl-*a* L^{-1} was used.

The images with NDCI>0 values were atmospherically corrected using the Dark Fit Spectrum method. In addition, an NDCI raster was generated for each image just for water pixels. To do so, cloud and land masking was performed using ACOLITE software (Vanhellemont and Ruddick, 2016). This generic processor was chosen because it was specifically developed for use in coastal and inland waters. Moreover, it is in

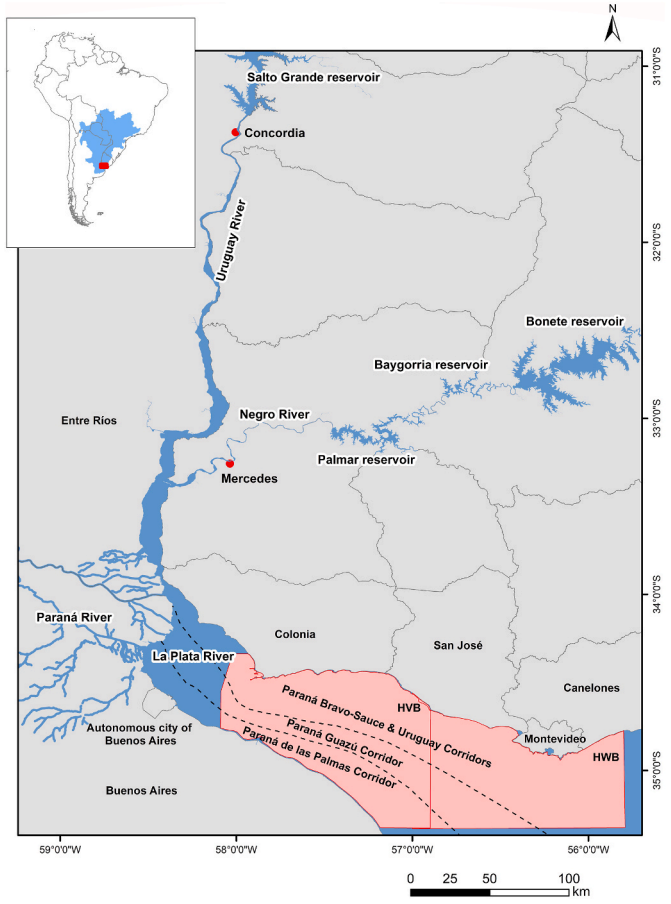

Fig. 2. Study area. Top left: La Plata basin (light blue) study area (red polygon). Main map: Work polygons identified with their grid codes HVB and HWB for Sentinel-2 images, flow recording stations (red dots), including a site on the Paraná River in the city of Rosario (32°58′22.04″S, 60°37′5.50″W) Argentina (not shown), and hydrological corridors (dotted line). (For interpretation of the references to color in this figure legend, the reader is referred to the Web version of this article.)

constant use, updating, and validation in several aquatic ecosystems (Ansper, 2018;Llori et al., 2019).

In order to determine the estuarine zones with the highest bloom occurrence, a frequency map was generated according to Maciel et al. (2021). To do so, the areas with high Chl-*a* concentration on each date were obtained by extracting the NDCI>0 values using the NDCI raster generated with ACOLITE. Once the NDCI>0 pixels were extracted, the monthly medians were calculated with the ArcMap Cell Statistics tool. Then the monthly medians were reclassified and a value of 1 was assigned to all the pixels. An image was then obtained for each month only with the pixels where a high Chl-*a* concentration was detected. Highest Chl-*a* concentration pixels were summed up for all the months with information, and each pixel was given a percentage value of high Chl-*a* concentration occurrence, for which the total number of months (57) of the period November 2016–July 2021 was considered as 100%. Then the procedure was repeated to obtain the seasonal and annual totals of the study period. The satellite information was processed using ArcMap 10.4.1 software.

In order to evaluate the effect of flow on blooms, the main areas with a high bloom occurrence were defined using the total frequency map previously developed. Polygons were generated to delimit the areas with a frequency greater than 25% in consolidated pixel clusters. These polygons were used to extract the median and the area corresponding to the pixels with NDCI>0 on each date with available images. A proxy for bloom size was then used as a response variable, which was obtained by

multiplying the area by the NDCI (median) of each image.

2.3. Bayesian hierarchical modeling framework

To estimate the effect of flow rate on bloom size (Yij), a hurdle model was used, which consists of a logistic model followed by a lognormal distribution, due to the large number of zeros found in the 4 zones (absence of blooms, Fig. S1). The logistic part of the model predicts the absences, while the lognormal part predicts the presences. Two flow rates were used as explanatory variables: The Paraná River (RP), on the one hand, and the Uruguay River plus the Negro River (RURN), on the other, which were considered together for being part of the same basin (Fig. 2). To summarize the conditions close to the capture area of the satellite data, the average flow rate of the last 3 days before each available image was used. To account for the seasonal effects expected for the study area, data were classified according to the thermal periods (high and low). To consider the differences between years, a random variable for the year was incorporated. The model can be expressed as follows:

$$p_{ij} \sim \text{Bernoulli}\ (\varphi_{ij})$$

$$\text{logit}(\varphi_{ij}) = \alpha_0 + \alpha_1 x_{1ij} + \alpha_2 x_{2ij} + \ldots + \alpha_k x_{kij} + \eta_{j1}$$

$$(Y_{ij}|Y_{ij}>0) \sim \text{LogNormal}\ (\mu_{ij,}\ \sigma^2)$$

$$\mu_{ij} = \beta_0 + \beta_1 x_{1ij} + \beta_2 x_{2ij} + \ldots + \beta_k x_{kij} + \eta_{j2}$$

where j = 1–5 year, i = 1 to 495 observations, and 1 to k covariates. The αs are the regression parameters in the logistic model, and the βs the regression parameters in the linear model. Random parameters η_{j1} and η_{j2} are the effects associated with the years in the logistic and the lognormal model, respectively. The covariates included in both regressions were river discharge for RP and RURN and their interactions with the categorical variable "bloom zone" (Z1-Z4) and the annual thermal cycle was divided into warm (high temperature, HT: November–April) and cold (low temperature, LT: May–October) periods. The model was adjusted using the brms package (Bürkner, 2017). Subsequent predictive controls were conducted to examine the model fit (McElreath, 2016). The model was then used to obtain predictions of the mean bloom size due to river discharge for each zone. First predictions were carried out varying RP river discharge in the range of our data, while RURN discharge value remained fixed. The same procedure was applied with an RP fixed value and a varying RURN value. For all the subsequent predictions, the random effect was set to zero. All covariates were standardized and assigned weekly informative priors, the default of the brms package. These priors make the null assumption that none of the covariates has an effect but includes a standard deviation that is broad enough to detect the effects of the standardized variables (Gelman, 2019). We ran 4 MCMC (Markov chains) each with 10000 iterations, and discarded 3000 (warm up) to obtain a total of 28000 samples from the distribution. Convergence was assessed using chain traceplots and calculating Rubin-Gelman statistics for each parameter, which were all below 1.1 (Gelman et al., 2014). Statistical analyses were performed in the R environment (R Core Team, 2020).

3. Results

3.1. Acquisition of satellite images

A total of 250 MSI/Sentinel-2 images were downloaded, 106 of which belonged to the HWB grid and 144 to the HVB grid. The number of images obtained increased progressively on an annual basis. Eight images were censored between November and December 2016, 40 images in 2017, 57 in 2018, 52 in 2019. In 2020, the annual maximum reached 61 images. Finally, between January and July 2021, 32 images were downloaded.

Most of the images acquired without cloud cover were censored between November and March. January was the month with the highest number of images downloaded with a total of 33 images, followed by November with 31 and December with 28. Conversely, the lowest number of cloud-free images was obtained in winter, August accounting for the minimum number, 11, followed by July as few as 12 images.

High concentrations of Chl-*a* were identified in the downloaded images. All the images captured in February showed pixels with NDCI values > 0, while NDCI values > 0 were 92% in March. Other high percentages were identified in December with 89% and in January with 82%. On the other hand, the months with the lowest percentage of occurrence were August with 36% and June with 47%. Elevated Chl-*a* concentrations were detected in 92% of the images censored during 2020, while, in 2017, the figure dropped to 53%.

3.2. Spatial-temporal distribution of phytoplankton blooms

During the study period, a progressive increase in the surface area and intensity of the NDCI indicator was identified during the warm period of the year (Nov–Apr) corresponding to El Niño phase (2018–2019). NDCI>0 pixels were found mainly towards the boundary with the outer estuarine zone where blooms reach the Montevideo coasts. The areas covered by intense blooms (NDCI>0.06) totaled 241 and 195 km^2 in February and January 2019, respectively, according to the monthly medians (Fig. 3).

During La Niña phase, the blooms were mainly located in the middle zone and towards the inner estuarine area, where they reached the greatest extent and intensity in the warm period from November to April. In the November 2019–April 2020 period, an increase in the area with intense blooms (NDCI>0.06) was detected, mainly located on the Uruguayan coast, covering 300 and 310 km^2 in January and March 2020, respectively. Between November 2020–April 2021, the blooms were also located in the inner estuarine zone, where they consolidated their prevalence on the Uruguayan coasts. High NDCI values were also recorded on the Argentine coasts. This period accounted for the largest areas with intense blooms. The maximum value recorded occurred in November 2020, followed by January 2021, with 515 and 474 km^2, respectively (Fig. 3).

During the study period, the daily mean flow of the RP, RU, and RN were 16313, 4195 and 826 m^3s^{-1}, respectively. The flows of the three rivers presented decreasing trends according to the Mann-Kendall test. The maximum flows recorded correspond chiefly to June–July 2017 where RP and RU reached daily values of up to 35677 and 25963 m^3s-^{1} respectively. In January–February 2019 maximum values of 34668 m^3s^{-1} in RP and 25270 m^3s^{-1} in RU were also recorded under El Niño conditions. On the other hand, the minimum daily flows of RP reached up to 6792 m^3s^{-1} during June–July 2021. In November 2020, some records accounted for just 7250 and 1052 m^3s^{-1} in RP and RU, respectively, between April–May 2020, and RU yielded minimum flows of up to 1064 m^3s^{-1} (Fig. 3). These low flow periods are explained by a weak to moderate La Niña period since July 2020.

3.3. Analysis of phytoplankton bloom frequency

The frequency with which phytoplankton blooms occurred in coastal areas increased progressively on both the Uruguayan and Argentine coasts. In particular, 2017 is the only year when a frequency higher than 25% was detected towards the inner estuarine zone and was not accompanied by similar frequencies in coastal areas. In 2019, a frequency higher than 25% in coastal areas stands out. Overall, 2017 and 2019 were the only years when zones with blooms close to Montevideo were detected in more than 25% of the study months. In 2020, the zone where the frequency was greater than 25% reached the largest area in the entire study period. Even though it decreased in 2021, this zone maintained a similar shape. Only in 2019, 2020, and 2021, areas above 75% of occurrence were recorded, and they were always found on the

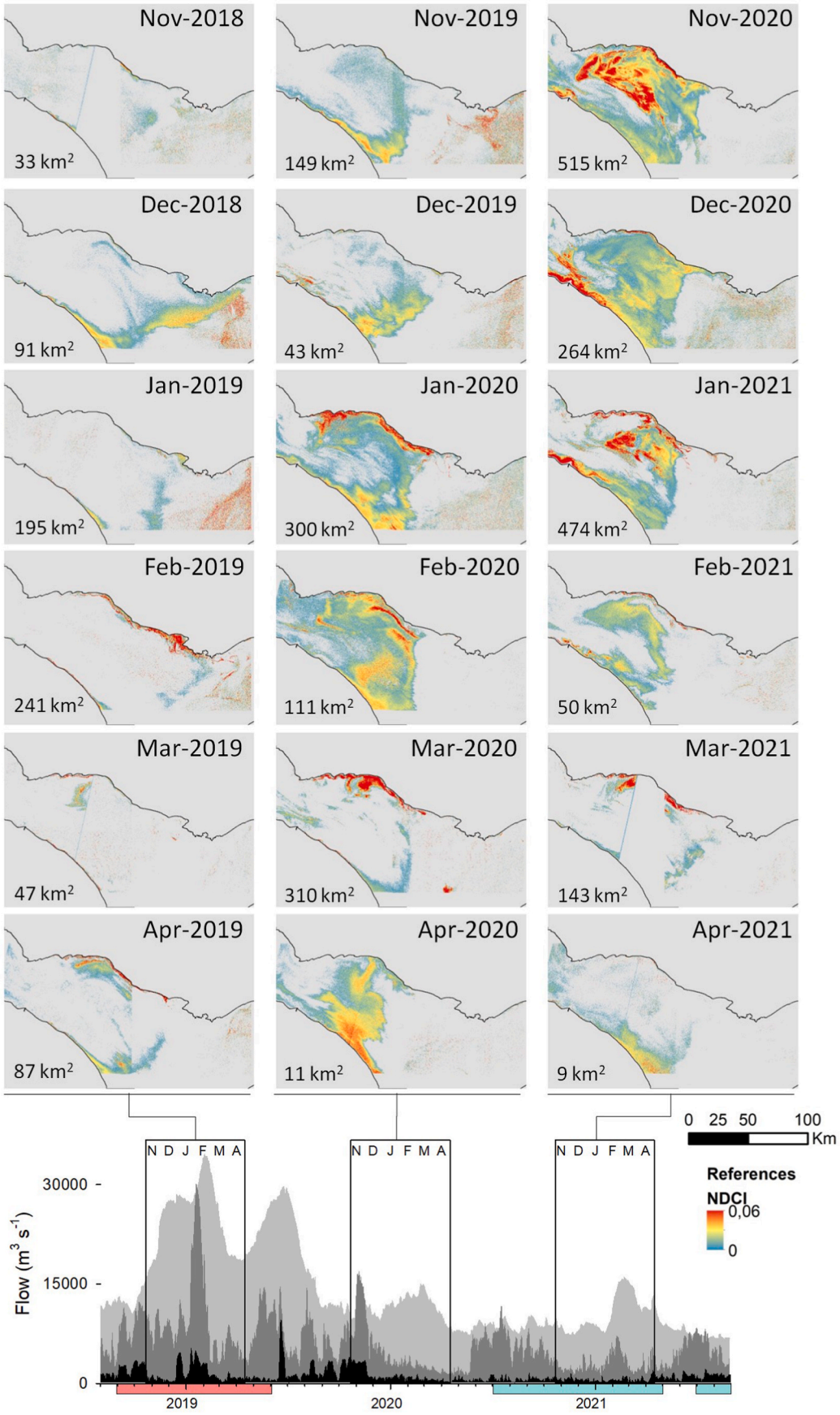

Fig. 3. NDCI monthly median in the warm months (November–April) in the middle and outer zone of the Río de la Plata during El Niño and La Niña phases (below: pink and light blue bars, respectively, delimited by the Oceanic Niño Index values greater or less than 0.5). Daily flow of the Paraná (light gray), Uruguay (dark gray) and Negro (black) rivers, measured at the Rosario, Concordia, and Mercedes stations, respectively. Note that the flow of the Uruguay River includes the flow of the Negro River (RURN). (For interpretation of the references to color in this figure legend, the reader is referred to the Web version of this article.)

coast of Buenos Aires Province (Fig. 4).

Bloom frequency is higher during the warm period of the year in the entire study area. This seasonal trend stands out for its high Chl-*a* concentration in more than 75% of the months under study on the Argentine coast. In turn, on the Uruguayan coast, elevated Chl-*a* concentrations reach frequencies higher than 50% with a wide area above 25% towards the inner Estuary in front of the Uruguayan coast. On the other hand, in the cold thermal period, blooms occur less frequently and are located in spatially confined areas. In addition, this period is characterized by a wide area located on the Uruguayan coast with frequencies higher than 25%, which, unlike the warm thermal period, reaches the Montevideo coast (Fig. 5).

During the months under study (57), the highest bloom episodes of the entire Estuary were detected in the coastal areas. The Argentine coast yielded frequencies above 25% along all its extension, while the Uruguayan coast in most of its part. The maximum frequencies identified were between 50 and 75% and reached 87 and 39.5 km on the Argentine and Uruguayan coasts, respectively. Towards the inner Estuary, blooms occurred less frequently. However, from the Argentine coast towards the inner Estuary the frequency decreased progressively, while towards the outer estuarine zone the pixels of intermediate frequency (25–50%) reached a larger area away from the coast. Westward the frequency above 25% remained close to the coast.

The frequency analyses allowed us to identify four zones where phytoplankton blooms occur in more than 25% of the months under study (Fig. 6). In total, Zone 1 is the one with the highest frequency with episodes during 50–75% of the months. It is followed by Zone 2, where pixels between 25-50% and 50–75% were detected. Zone 4 presents the same frequencies and is characterized by being the narrowest. As for the inner estuarine zones, Zone 3 is formed by a dense cluster of pixels between 25 and 50% and with some scattered pixels between 50 and 75% (Fig. 6).

3.4. Effect of flow on the zones with the highest bloom frequency

The Bayesian model indicated clear effects of river flow on bloom size evidenced by the observed slopes (Fig. 7) and the estimated standardized coefficients (Fig. S2). In particular, the increased RP flow for the 4 zones was found to have a negative effect on Zone 2 and, to a lesser extent, on Zone 1. In turn, increased RURN flow had a negative effect on bloom size in Zone 3 and, to a lesser extent, in Zone 4 (Fig. 7, Fig. S2). Along these lines, the probability of absence (no bloom) raises with an increasing flow rate, the response being different between the warm and the cold periods (Fig. S3).

4. Discussion

The temporal and spatial analysis of elevated Chl-*a* concentrations allowed us to identify four zones of high frequency of phytoplankton bloom occurrence in the intermediate RdlP, as well as its association with the flow variations of the main tributary rivers under El Niño and La Niña climate conditions. It was possible to determine that the highest phytoplankton biomass occur in the northern and southern coastal areas in the warmer months, although with greater intensity and extent on the Argentine coast. This is to be expected since, according to Silva et al. (2014), the location of the saline front varies the most in the area near the Uruguayan coast and is affected by flow rates and winds. In any case, the phenomenon can extend to inland waters independently of the season. The transport resulting from high RP and RURN flows tends to affect the presence of blooms at a general level, although with high spatially restricted coastal accumulations (e.g., 2019 bloom on the Uruguayan coast, Aubriot et al., 2020), while low flows favor the

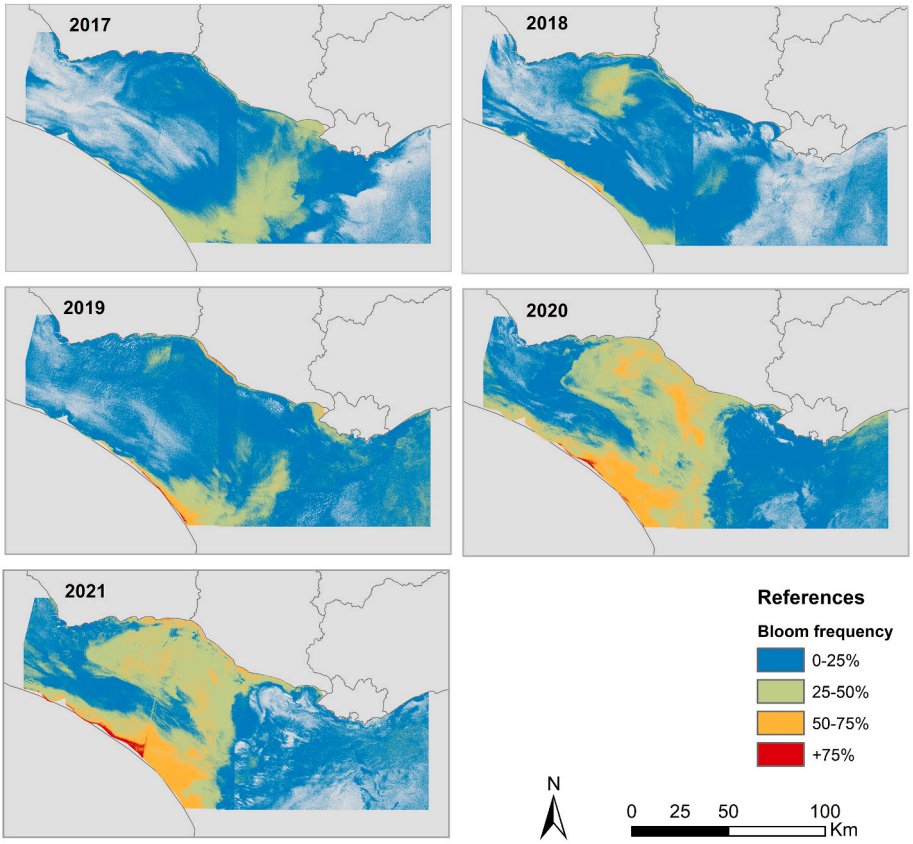

Fig. 4. Annual frequency of phytoplankton bloom occurrence in the middle and outer zone of the Río de la Plata, according to the annual sum of the monthly median of pixels with NDCI values greater than 0 over the total number of months per year.

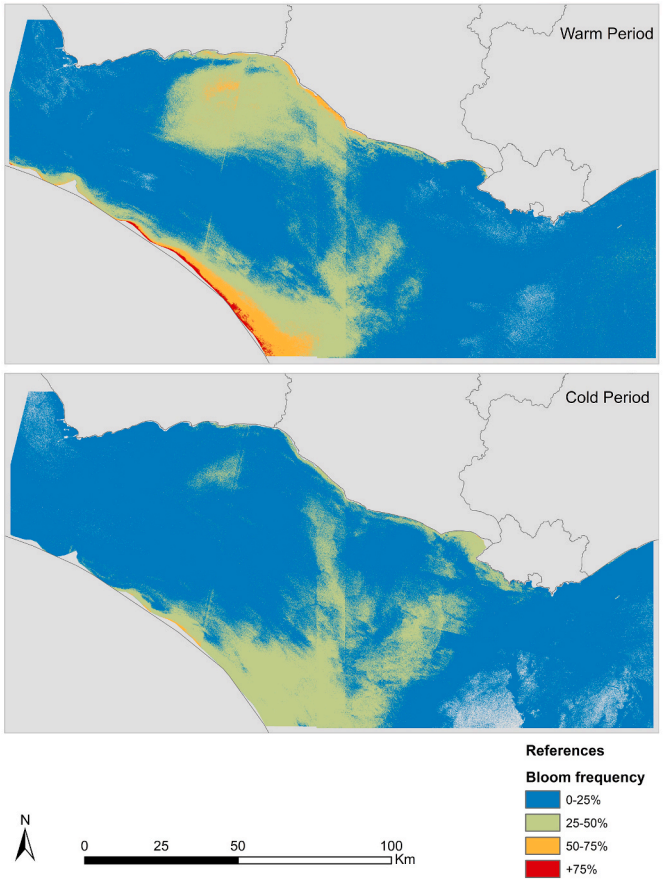

Fig. 5. Frequency of phytoplankton bloom occurrence according to the thermal periods (cold vs warm) shown as the sum of the monthly median of pixels with NDCI values > 0 over the total months per thermal period.

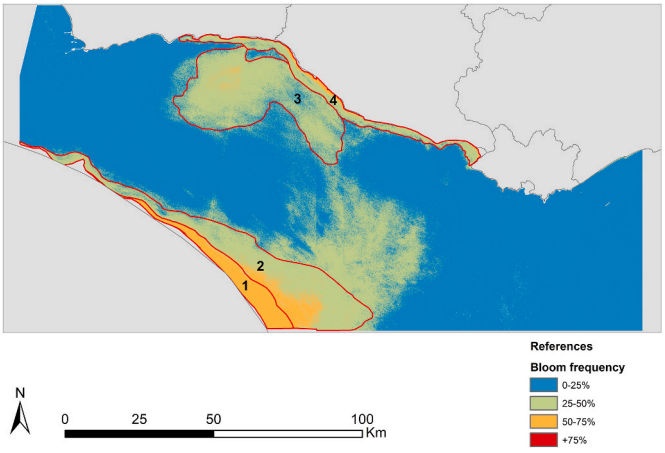

Fig. 6. Total frequency of phytoplankton bloom occurrence according to the total sum of monthly median of pixels with NDCI values > 0 over the total months of the study period and numbered zonation (in red). Area (km^2): Zone 1, 289; Zone 2, 985; Zone 3, 1101; and Zone 4, 311. (For interpretation of the references to color in this figure legend, the reader is referred to the Web version of this article.)

development of extensive blooms. This work identified a recurrent pattern of phytoplankton blooms in specific areas of the RdlP and the conditions that favor their magnification, linked to the hydro-meteorological variability of the region. The results obtained allowed us to advance in the prediction of this phenomenon in a context of strong climate variability in the region and worrying levels of estuarine eutrophication.

In the warmer months, blooms recorded *in situ* on the northern and southern shores of the RdlP are generally produced by cyanobacteria, particularly those belonging to the *Microcystis aeruginosa* (MAC) complex. Records of toxic blooms of MAC on the northern coast are more than two decades old, ranging from the inner zone of the RdlP (Colonia) to the beaches of Montevideo (De Leon and Yunes, 2001; Pírez et al., 2013; Haakonsson et al., 2020). When MAC complex blooms take place in the turbidity front and up to the outer limit of the Estuary, they typically occur when freshwater conditions prevail due to high river flows (Haakonsson et al., 2020). In the warm period and low river flows, the salinity front enters from the northeast (FREPLATA, 2005), limiting the advance of the blooms of zone 4 along the north coast. On the southern coast, the first records of these blooms correspond to the same decade, mainly on the coast of La Plata (Andrinolo et al., 2007; Sathicq et al., 2014). In the cold period, including spring, the composition of the blooms recorded is attributed to eukaryotic phytoplankton, particularly diatoms and dinoflagellates, which can reach the outer limit of the Estuary (Carreto et al., 2003; Calliari et al., 2005). These blooms usually accompany the saline front that advances towards the open sea (FREPLATA, 2005). Nonetheless, the presence of *Microcystis* in low biomass prevails during the winter in both margins and under low salinity conditions (Andrinolo et al., 2007). It is noteworthy that most of the information available on cyanobacteria blooms in the RdlP is mainly coastal. This makes it difficult to evaluate their behavior and taxonomic composition inside the Estuary. Considering that sampling in the Estuary requires high operational costs, our work allowed us to identify areas of phytoplankton bloom occurrence as an input for sampling design and the definition of reference monitoring stations. It should be noted that most of the clear images were from the warm season, which can generate some biases.

According to this study, the location of high NDCI values was always behind the turbidity front. In addition, the spatial distribution of the blooms identified for the Uruguayan coast was as expected according to Dogliotti et al. (2016), who reported that the Uruguayan coast had lower turbidity and less seasonal variation than the Argentine coast, except for the autumn months when turbidity increased on both margins. However, the area to the west of Montevideo maintains low turbidity levels throughout all months compared to the rest of the Estuary (Maciel et al., 2021). Light penetration through the water column along with longer residence times and nutrient availability would be the most relevant factors for the development of phytoplankton blooms in the RdlP Estuary (Nagy et al., 2002). Also, turbidity caused by inorganic solids may act as a strong regulator of phytoplankton productivity at the turbidity front (Kruk *et al.*, 2015). On the other hand, Moreira et al. (2013) postulated that material discharge derives mainly from the Paraná River. Therefore, the Paraná Bravo-Sauce and Uruguay corridors present the lowest turbidity, which could favor phytoplankton growth in zones 3 and 4 (Fig. 6). In addition, these zones are located in regions with larger suspended materials according to Piedra-Cueva and Fossati (2007). Given the high levels of nutrients present in the Estuary, temperature, lower turbidity, and longer water residence times would be key factors for the development of HABs.

According to satellite monitoring, bloom occurrence varies between the years evaluated and is related to variations in estuarine flow rates, which, as indicated by Nagy et al. (2002), Sathicq et al. (2014), and Brugnoli et al. (2020), are regulated by large-scale phenomena such as the El Niño- Southern Oscillation event. Along the period under study, and during El Niño phase, blooms were restricted to the northern coast and more frequently took place on Montevideo coasts. These results are in line with those by Brugnoli et al. (2019) and the report by Risso et al. (2021) who arrived at such conclusion after analyzing data from water quality monitoring of Montevideo beaches conducted from 2000 to 2021. In this sense, López and Nagy (2005) suggested that the massive phytoplankton bloom recorded on the Uruguayan coast during the

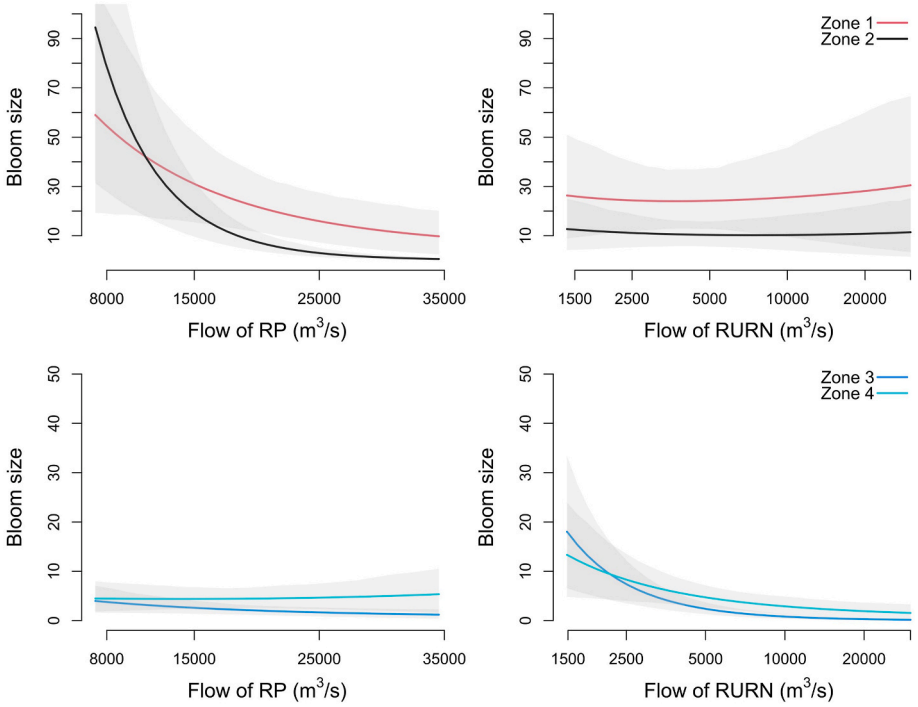

Fig. 7. Successive predictive distribution of bloom size as a function of the Río Parana (RP) and Uruguay-Negro rivers (RURN) flow (m^3/s) by zone (1–4) for the warm period. Note that the Y axis corresponds to the product between NDCI and bloom area (pixels NDCI >0).

2002–2003 was favored by the great flooding of the RU. Likewise, some earlier studies claim that the massive blooms recorded in Montevideo are linked to the high flows of the RU transporting biomass from hydroelectric reservoirs, in particular Salto Grande (Kruk et al., 2019). However, recently Aubriot et al. (2020) identified from satellite images that the hydroelectric reservoirs of the RN were the main magnifiers of large cyanobacterial biomass discharged downstream based on the sharp increase in flow, as it happened in the austral summer of 2019 during El Niño phase.

According to the results obtained in our study, high RURN flows favor bloom occurrence on the northern coast. However, they correspond to blooms of a smaller extent than in La Niña events, at the level of the rest of the Estuary. Likewise, according to the Bayesian model performed in this study, low RURN flows boost large biomass development in zones 3 and 4 (Fig. 6). This phenomenon could be facilitated by the increase in freshwater residence time due to low flows, together with the easterly winds characteristic of summer (Barreiro et al., 2021). Therefore, large phytoplankton biomass would develop in zones 3 and 4, which move towards Montevideo city in sporadic events when the flow increases. In this sense, despite the fact that the literature sustains that the blooms recorded in Montevideo are positively associated with RURN flows, this study shows that the general pattern at the intermediate Estuary level is one of biomass decrease in periods of high flows and that the blooms do not exclusively come from the reservoirs located upstream. Estuarine eutrophication, in combination with low flows, leads to the greatest extensions of phytoplankton biomass, particularly of toxic cyanobacteria of the *Microcystis* complex.

This work showed a progressive increase in the annual frequency of phytoplankton blooms in the middle Estuary during an extreme drought in La Plata basin (Naumann et al., 2021), which produced a historically low RP. In general terms, blooms increase in frequency and extent during warmer months, and are concentrated in coastal and inland estuarine areas. This phenomenon was evidenced both in the frequency mapping (Fig. 5) as well as in the modeling performed, which showed a negative ratio between RP and RURN flow rates and bloom size in zones 1 and 2, and zones 3 and 4, respectively (Fig. 7). These results coincide with those obtained by Nagy et al. (2002) in the 1990s. The authors reported that cyanobacterial blooms could develop during the summer season, particularly in the so-called Eastern Channel, located on the northern coast and in the inner and middle Estuary, because the reduction of freshwater inflow increased the residence time and boosted phytoplankton development. Likewise, Sathicq et al. (2014) indicated that during La Niña phase, the concentration of Chl-*a* raised in the Argentine coasts with respect to the neutral and El Niño periods. Increased precipitation and flows in La Plata basin are expected for the coming decades (Allan et al., 2021), with the consequent deleterious socioeconomic and environmental impacts due to the effect of cyanobacteria blooms along the Uruguayan coast. However, the environmental impact of prolonged droughts such as the current one (three consecutive years of La Niña) could continue to deteriorate the estuary's water quality, with negative consequences on production and aquatic biodiversity. The trends due to climate change for the RdlP region indicate increases in interannual rainfall (Barreiro et al., 2019), the frequency of occurrence and intensity of droughts in the region and winds from the East component in the RdlP (Barreiro et al., 2021). According to our findings, these changes in the dynamics of the Estuary will have effects on bloom's frequency and size. Having a continuous monitoring strategy with remote sensing techniques allows obtaining information to model some effects of climate change in the RdlP.

The identification of areas with high frequency of phytoplankton blooms, along with their temporal dynamics, is of particular importance for Estuary management. For instance, it allows to identify and anticipate, on a spatial and temporal basis, the scenario of phytoplankton bloom occurrence in the context of future activities planned in the Estuary. In particular, the construction of a water purification plant is currently planned to supplement water supply to Montevideo city, which would be located in the middle of Zone 4 (Fig. 6). The results of this work allowed us to identify that the water quality at that site would not be suitable for treatment during the summer during both La Niña and El Niño years. On the other hand, the discharge of urban effluents from Buenos Aires city is expected to begin through an outfall located 12 km away from the coast (zones 1 and 2). Such discharge outfall would

have a direct effect on nutrient and organic matter contribution at the start of zones 1 and 2. Both projects, with opposing uses of the Estuary, will be located at the sites with a maximum frequency of phytoplankton blooms, particularly of cyanobacteria.

5. Conclusions

In the known context of RdlP eutrophication, this study shows that phytoplankton blooms can develop massively in specific estuarine zones, and that they are regulated by contrasting weather processes. Four zones of high frequency of bloom occurrence were delimited, providing a new scenario on the spatial and temporal dynamics of phytoplankton blooms in the RdlP and their relationship with flow rates. These results contribute to the advancement of the prediction of this phenomenon in a context of strong climate variability. The mapping of zones with high frequency of phytoplankton blooms also has consequences for management of the estuary. For example, large urban sewage effluents, that can worsen the bloom formation, and water intakes that can hamper drinking water production, may have a larger environmental impact and/or pose health risks if located close to a high frequency HAB zone. In addition, efforts in controlling eutrophication in both main tributaries are needed to impact in the bloom formation in the Estuary, particularly in the identified high frequency zones. In this framework, future studies should focus on evaluating the specific physicochemical characteristics of the zones identified in this study in order to contribute to the development of predictive models.

During periods of low flow, the Estuary increases its residence time and facilitates the development of extensive and high-intensity blooms in the Uruguayan coastal and inland estuarine areas, which may occasionally be transported to Montevideo. When RURN flows increase, blooms are generally strongly restricted to Zone 4, and may be transported beyond the coast of Montevideo. This confirms the postulates that indicate a positive ratio between RURN flows and blooms on Montevideo beaches. As for the Argentine coast, the higher frequency and intensity of blooms were negatively related to RP flow, reaching maximums in extent and intensity during the recent historical low flow of the river. These results highlight the effects of strong eutrophication pressures on the Estuary and the key role that extreme climate events play and that are expected to increase in intensity, as well as the great current environmental vulnerability of RdlP.

CRediT authorship contribution statement

Bernardo Zabaleta: Writing – review & editing, Writing – original draft, Visualization, Methodology, Investigation, Funding acquisition, Formal analysis, Conceptualization.

Declaration of competing interest

The authors declare the following financial interests/personal relationships which may be considered as potential competing interests: Bernardo Zabaleta reports financial support was provided by Sectoral Commission for Scientific Research of the University of the Republic.

Data availability

Data will be made available on request.

Acknowledgements

We especially thank María de la Paz Oteiza for valuable linguistic corrections. The research was funded by the Sectoral Commission for Scientific Research of the University of the Republic through the project INI (2019) N° 360.

Appendix A. Supplementary data

Supplementary data to this article can be found online at https://doi.org/10.1016/j.ecss.2023.108342.

References

Acha, E.M., Mianzan, H., Guerrero, R., Carreto, J., Giberto, D., Montoya, N., Carignan, M., 2008. An overview of physical and ecological processes in the Rio de la Plata Estuary. Continent. Shelf Res. 28 (13), 1579–1588.
Allan, R.P., Hawkins, E., Bellouin, N., Collins, B., 2021. IPCC, 2021: Summary for Policymakers.
Anderson, D.M., Andersen, P., Bricelj, V.M., Cullen, J.J., Rensel, J.J., 2001. Monitoring and Management Strategies for Harmful Algal Blooms in Coastal Waters. Unesco, Paris, France, p. 268.
Andrinolo, D., Pereira, P., Giannuzzi, L., Aura, C., Massera, S., Caneo, M., et al., 2007. Occurrence of *Microcystis aeruginosa* and microcystins in Río de la Plata river (Argentina). Acta toxicólogica argentina 15 (1), 8–14.
Aubriot, L., Zabaleta, B., Bordet, F., Sienra, D., Risso, J., Achkar, M., Somma, A., 2020. Assessing the origin of a massive cyanobacterial bloom in the Río de la Plata (2019): towards an early warning system. Water Res. 181, 115944.
Augusto-Silva, P.B., Ogashawara, I., Barbosa, C.C., De Carvalho, L.A., Jorge, D.S., Fornari, C.I., Stech, J.L., 2014. Analysis of MERIS reflectance algorithms for estimating chlorophyll-a concentration in a Brazilian reservoir. Rem. Sens. 6 (12), 11689–11707.
Ansper, A., 2018. SENTINEL-2/MSI APPLICATIONS FOR EUROPEAN UNION WATER FRAMEWORK DIRECTIVE REPORTING PURPOSES.
Barreiro, M., Arizmendi, F., Díaz, N., Trinchin, R., 2021. Análisis de la variabilidad y tendencias observadas de los vientos en Uruguay.
Barreiro, M., Trinchin, R., Arizmendi, F., 2019. Proyecciones del clima sobre Uruguay. Informe Plan Nacional de Adaptación para la zona costera. https://www.gub.uy/ministerio-ambiente/plan-nacional-adaptaci%C3%B3n-zona-costera. Available in:
Beck, R., Zhan, S., Liu, H., Tong, S., Yang, B., Xu, M., et al., 2016. Comparison of satellite reflectance algorithms for estimating chlorophyll-a in a temperate reservoir using coincident hyperspectral aircraft imagery and dense coincident surface observations. Rem. Sens. Environ. 178, 15–30.
Bowling, L.C., Blais, S., Sinotte, M., 2015. Heterogeneous spatial and temporal cyanobacterial distributions in Missisquoi Bay, Lake Champlain: an analysis of a 9 year data set. J. Great Lake. Res. 41 (1), 164–179.
Brugnoli, E., Muniz, P., Venturini, N., Brena, B., Rodríguez, A., García-Rodríguez, F., 2019. Assessing multimetric trophic state variability during an ENSO event in a large estuary (Río de la Plata, South America). Regional Studies in Marine Science 28, 100565.
Brugnoli, E., Arocena, R., Cabrera-Lamanna, L., Muniz, P., 2020. Management and Monitoring of Eutrophication: Trophic State Indexes on the Río de la Plata Northern Coast. Life Below Water, pp. 1–13.
Burford, M.A., Carey, C.C., Hamilton, D.P., Huisman, J., Paerl, H.W., Wood, S.A., Wulff, A., 2020. Perspective: advancing the research agenda for improving understanding of cyanobacteria in a future of global change. Harmful Algae 91, 101601.
Bürkner, P.C., 2017. brms: an R package for Bayesian multilevel models using Stan. J. Stat. Software 80, 1–28.
Caballero, I., Fernández, R., Escalante, O.M., Mamán, L., Navarro, G., 2020. New capabilities of Sentinel-2A/B satellites combined with in situ data for monitoring small harmful algal blooms in complex coastal waters. Sci. Rep. 10 (1), 1–14.
Calliari, D., Gómez, M., Gómez, N., 2005. Biomass and composition of the phytoplankton in the Río de la Plata: large-scale distribution and relationship with environmental variables during a spring cruise. Continent. Shelf Res. 25 (2), 197–210.
Camilloni, I., Barros, V., 2000. The Parana river response to El Nino 1982–83 and 1997–98 events. J. Hydrometeorol. 1 (5), 412–430.
Carpenter, S.R., Caraco, N.F., Correll, D.L., Howarth, R.W., Sharpley, A.N., Smith, V.H., 1998. Nonpoint pollution of surface waters with phosphorus and nitrogen. Ecol. Appl. 8 (3), 559–568.
Carreto, J.I., Montoya, N.G., Benavides, H.R., Guerrero, R., Carignan, M.O., 2003. Characterization of spring phytoplankton communities in the Río de La Plata maritime front using pigment signatures and cell microscopy. Mar. Biol. 143 (5), 1013–1027.
Chapin III, F.S., Matson, P.A., Vitousek, P., 2011. Principles of Terrestrial Ecosystem Ecology. Springer Science & Business Media.
Chorus, I., Welker, M., 2021. Toxic Cyanobacteria in Water: a Guide to Their Public Health Consequences, Monitoring and Management. Taylor & Francis, p. 858.
Conley, D.J., Paerl, H.W., Howarth, R.W., Boesch, D.F., Seitzinger, S.P., Havens, K.E., Likens, G.E., 2009. Controlling eutrophication: nitrogen and phosphorus. Science 323 (5917), 1014–1015.
De Leon, L., Yunes, J.S., 2001. First report of a microcystin-containing bloom of the cyanobacterium *Microcystis aeruginosa* in the La Plata River, South America. Environ. Toxicol.: Int. J. 16 (1), 110–112.
Dodds, W.K., Bouska, W.W., Eitzmann, J.L., Pilger, T.J., Pitts, K.L., Riley, A.J., et al., 2009. Eutrophication of US Freshwaters: Analysis of Potential Economic Damages.
Dogliotti, A.I., Ruddick, K., Guerrero, R., 2016. Seasonal and inter-annual turbidity variability in the Río de la Plata from 15 years of MODIS: El Niño dilution effect. Estuar. Coast Shelf Sci. 182, 27–39.

Dörnhöfer, K., Klinger, P., Heege, T., Oppelt, N., 2018. Multi-sensor satellite and in situ monitoring of phytoplankton development in a eutrophic-mesotrophic lake. Sci. Total Environ. 612, 1200–1214.
Framiñan, M.B., Brown, O.B., 1996. Study of the Río de la Plata turbidity front, Part 1: spatial and temporal distribution. Continent. Shelf Res. 16 (10), 1259–1282.
Freplata, 2005. Análisis diagnóstico transfronterizo del Río de la Plata y su Frente Marítimo. Documento técnico. Proyecto Protección Ambiental del Río de la Plata y su Frente Marítimo, p. 301. Proyecto PNUD/GEF/RLA/99/G31.
Gallegos, C.L., Neale, P.J., 2015. Long-term variations in primary production in a eutrophic sub-estuary: contribution of short-term events. Estuar. Coast Shelf Sci. 162, 22–34.
García-Alonso, J., Lercari, D., Defeo, O., 2019. Río de la Plata: a neotropical estuarine system. In: Coasts and Estuaries. Elsevier, pp. 45–56.
Gelman, A., Carlin, J., Stern, H., Dunson, D., Vehtari, A., Rubin, D.B., 2014. Bayesian Data Analysis, 3 edition. CRC Press, Boca Raton.
Gelman, A., 2019. Prior choice recommendations. Stan-dev/stan. GitHub.
Giannuzzi, L., Carvajal, G., Corradini, M.G., Araujo Andrade, C., Echenique, R., Andrinolo, D., 2012. Occurrence of toxic cyanobacterial blooms in Rio de la Plata Estuary, Argentina: field study and data analysis. J. Toxicol. 2012.
Gitelson, A.A., Nikanorov, A.M., Szabo, G.Y., Szilagyi, F., 1986. Etude de la qualite des eaux de surface par teledetection. IAHS-AISH publication, pp. 111–121, 157.
Gitelson, A., 1992. The peak near 700 nm on radiance spectra of algae and water: relationships of its magnitude and position with chlorophyll concentration. Int. J. Rem. Sens. 13 (17), 3367–3373.
Gómez, N., 2014. Phytoplankton of the Río de la Plata estuary. Freshwater Phytoplankton of Argentina, Advances in Limnology 65, 167–181.
Gons, H.J., Rijkeboer, M., Ruddick, K.G., 2002. A chlorophyll-retrieval algorithm for satellite imagery (Medium Resolution Imaging Spectrometer) of inland and coastal waters. J. Plankton Res. 24 (9), 947–951.
Gons, H.J., 1999. Optical teledetection of chlorophyll a in turbid inland waters. Environ. Sci. Technol. 33 (7), 1127–1132.
Gordon, H.R., Clark, D.K., Mueller, J.L., Hovis, W.A., 1980. Phytoplankton pigments from the nimbus-7 coastal zone color scanner: comparisons with surface measurements. Science 210 (4465), 63–66.
Haakonsson, S., Rodríguez, M.A., Carballo, C., del Carmen Perez, M., Arocena, R., Bonilla, S., 2020. Predicting cyanobacterial biovolume from water temperature and conductivity using a Bayesian compound Poisson-Gamma model. Water Res. 176, 115710.
Hardisty, J., 2007. Assessment of tidal current resources: case studies of estuarine and coastal sites. Energy Environ. 18 (2), 233–249.
Kruk, C., Martínez, A., Nogueira, L., Alonso, C., Calliari, D., 2015. Morphological traits variability reflects light limitation of phytoplankton production in a highly productive subtropical estuary (Río de la Plata, South America). Mar. Biol. 162 (2), 331–341.
Kruk, C., Martínez, A., de la Escalera, G.M., Trinchin, R., Manta, G., Segura, A.M., et al., 2019. Floración excepcional de cianobacterias tóxicas en la costa de Uruguay, verano 2019. Innotec (18), 36–68.
Kutser, T., Paavel, B., Verpoorter, C., Ligi, M., Soomets, T., Toming, K., Casal, G., 2016. Remote sensing of black lakes and using 810 nm reflectance peak for retrieving water quality parameters of optically complex waters. Rem. Sens. 8 (6), 497.
Lins, R.C., Martinez, J.M., Motta Marques, D.D., Cirilo, J.A., Fragoso Jr., C.R., 2017. Assessment of chlorophyll-a remote sensing algorithms in a productive tropical estuarine-lagoon system. Rem. Sens. 9 (6), 516.
Liu, H., Li, Q., Shi, T., Hu, S., Wu, G., Zhou, Q., 2017. Application of sentinel 2 MSI images to retrieve suspended particulate matter concentrations in Poyang Lake. Rem. Sens. 9 (7), 761.
López, C., Nagy, G., 2005. Cambio global, evolución del estado trófico y floraciones de cianobacterias en el Río de la Plata.*El cambio climático en el Río de la Plata.* CIMA, Buenos Aires, pp. 157–166.
Maciel, F.P., Santoro, P.E., Pedocchi, F., 2021. Spatio-temporal dynamics of the Río de la Plata turbidity front; combining remote sensing with in-situ measurements and numerical modeling. Continent. Shelf Res. 213, 104301.
McElreath, R., 2016. Rethinking: an R Package for Fitting and Manipulating Bayesian Models.
Michalak, A.M., 2016. Study role of climate change in extreme threats to water quality. Nature 535 (7612), 349–350.
Mishra, S., Mishra, D.R., 2012. Normalized difference chlorophyll index: a novel model for remote estimation of chlorophyll-a concentration in turbid productive waters. Rem. Sens. Environ. 117, 394–406.
Mishra, S., Mishra, D.R., 2014. A novel remote sensing algorithm to quantify phycocyanin in cyanobacterial algal blooms. Environ. Res. Lett. 9 (11), 114003.
Mishra, D., Ramaswamy, L., Kumar, A., Bhandarkar, S., Kumar, V., Narumalani, S., 2018. A multi-cloud cyber infrastructure for monitoring global proliferation of cyanobacterial harmful algal blooms. In: IGARSS 2018-2018 IEEE International Geoscience and Remote Sensing Symposium. IEEE, pp. 9272–9275.
Mitchell, S.B., Jennerjahn, T.C., Vizzini, S., Zhang, W., 2015. Changes to processes in estuaries and coastal waters due to intense multiple pressures–An introduction and synthesis. Estuar. Coast Shelf Sci. 156, 1–6.
Moreira, D., Simionato, C.G., Gohin, F., Cayocca, F., Tejedor, M.L.C., 2013. Suspended matter mean distribution and seasonal cycle in the Río de La Plata estuary and the adjacent shelf from ocean color satellite (MODIS) and in-situ observations. Continent. Shelf Res. 68, 51–66.
Muniz, P., Venturini, N., Brugnoli, E., Gutiérrez, J.M., Acuña, A., 2019. Río de la Plata: Uruguay. In: World Seas: an Environmental Evaluation. Academic Press, pp. 703–724.
Nagy, G.J., Gómez-Erache, M., López, C.H., Perdomo, A.C., 2002. Distribution patterns of nutrients and symptoms of eutrophication in the Rio de la Plata river estuary system. In: Nutrients and Eutrophication in Estuaries and Coastal Waters. Springer, Dordrecht, pp. 125–139.
Naumann, G., Podesta, G., Marengo, J., Luterbacher, J., Bavera, D., Arias-Muñoz, C., Marinho Ferreira Barbosa, P., Cammalleri, C., Chamorro, L., Cuartas, L.A., De Jager, A., Escobar, C., Hidalgo, C., Leal De Moraes, O.L., Mccormick, N., Maetens, W., Magni, D., Masante, D., Mazzeschi, M., Seluchi, M., De Los Milagros Skansi, M., Spinoni, J., Toreti, A., 2021. The 2019-2021 Extreme Drought Episode in La Plata Basin. EUR 30833 EN, Publications Office of the European Union, Luxembourg. https://doi.org/10.2760/773, 978-92-76-41898-6.
Navalgund, R.R., Jayaraman, V., Roy, P.S., 2007. Remote sensing applications: an overview. Curr. Sci. 1747–1766.
Nechad, B., Ruddick, K.G., Park, Y., 2010. Calibration and validation of a generic multisensor algorithm for mapping of total suspended matter in turbid waters. Rem. Sens. Environ. 114 (4), 854–866.
O'Neil, J.M., Davis, T.W., Burford, M.A., Gobler, C.J., 2012. The rise of harmful cyanobacteria blooms: the potential roles of eutrophication and climate change. Harmful Algae 14, 313–334.
Oliver, R.L., Hamilton, D.P., Brookes, J.D., Ganf, G.G., 2012. Physiology, blooms and prediction of planktonic cyanobacteria. In: Ecology of Cyanobacteria II. Springer, Dordrecht, pp. 155–194.
Page, B.P., Kumar, A., Mishra, D.R., 2018. A novel cross-satellite based assessment of the spatio-temporal development of a cyanobacterial harmful algal bloom. Int. J. Appl. Earth Obs. Geoinf. 66, 69–81.
Piedra-Cueva, I., Fossati, M., 2007. Residual currents and corridor of flow in the Rio de la Plata. Appl. Math. Model. 31 (3), 564–577.
Pírez, M., Gonzalez-Sapienza, G., Sienra, D., Ferrari, G., Last, M., Last, J.A., Brena, B.M., 2013. Limited analytical capacity for cyanotoxins in developing countries may hide serious environmental health problems: simple and affordable methods may be the answer. J. Environ. Manag. 114, 63–71.
R Core Team, 2020. R: A Language and Environment for Statistical Computing. R Foundation for Statistical Computing, Vienna, Austria. Available at: *https://www.R-project.org/*.
Risso, J., Sienra, D., D'Alessandro, B., Echezarreta, M.E., 2021. Programa de monitoreo de agua de playas y costa del departamento de Montevideo. 2021. In: -M, I.A.A. (Ed.), Intendencia de Montevideo. Servicio de Evaluación de Calidad y Control Ambiental Departamento de Desarrollo Ambiental, Montevideo, p. 68.
Ritchie, J.C., Zimba, P.V., Everitt, J.H., 2003. Remote sensing techniques to assess water quality. Photogramm. Eng. Rem. Sens. 69 (6), 695–704.
Sathicq, M.B., Gómez, N., Andrinolo, D., Sedán, D., Donadelli, J.L., 2014. Temporal distribution of cyanobacteria in the coast of a shallow temperate estuary (Río de la Plata): some implications for its monitoring. Environ. Monit. Assess. 186 (11), 7115–7125.
Schalles, J.F., Hladik, C.M., 2012. Mapping phytoplankton chlorophyll in turbid, Case 2 estuarine and coastal waters. Isr. J. Plant Sci. 60 (1–2), 169–191.
Silva, C.P., Marti, C.L., Imberger, J., 2014. Horizontal transport, mixing and retention in a large, shallow estuary: Río de la Plata. Environ. Fluid Mech. 14 (5), 1173–1197.
Smayda, T.J., 1998. Patterns of variability characterizing marine phytoplankton, with examples from Narragansett Bay. ICES (Int. Counc. Explor. Sea) J. Mar. Sci. 55 (4), 562–573.
Strong, A.E., 1974. Remote sensing of algal blooms by aircraft and satellite in Lake Erie and Utah Lake. Rem. Sens. Environ. 3 (2), 99–107.
Tamm, M., Ligi, M., Panksep, K., Teeveer, K., Freiberg, R., Laas, P., et al., 2019. Boosting the monitoring of phytoplankton in optically complex coastal waters by combining pigment-based chemotaxonomy and in situ radiometry. Ecol. Indicat. 97, 329–340.
Toming, K., Kutser, T., Laas, A., Sepp, M., Paavel, B., Nõges, T., 2016. First experiences in mapping lake water quality parameters with Sentinel-2 MSI imagery. Rem. Sens. 8 (8), 640.
Vanhellemont, Q., Ruddick, K., 2016. Acolite for sentinel-2: aquatic applications of MSI imagery. In: Proceedings of the 2016 ESA Living Planet Symposium, pp. 9–13. Prague, Czech Republic.